Research Article | Vol. 30, No. 25 / 5 Dec 2022 / Optics Express 45517
Optics EXPRESS

All-optical information conversion in Rb vapor based on the spatial cross-phase modulation

SANDAN WANG,[1,2] JINPENG YUAN,[1,2,3] LIRONG WANG,[1,2,*] LIANTUAN XIAO,[1,2] AND SUOTANG JIA[1,2]

[1]State Key Laboratory of Quantum Optics and Quantum Optics Devices, Institute of Laser Spectroscopy, Shanxi University, 92 Wucheng Road, Taiyuan 030006, China
[2]Collaborative Innovation Center of Extreme Optics, Shanxi University, 92 Wucheng Road, Taiyuan 030006, China
[3]yjp@sxu.edu.cn
*wlr@sxu.edu.cn

Abstract: All-optical information conversion, conveying optical signals without electro-optical transformation, plays a vital role in the all-optical devices and optical communication. We achieve the all-optical information conversion in Rb vapor by utilizing the spatial cross-phase modulation. The refractive index of atomic medium is spatially modulated by the strong switch laser beam, which makes it as a nonlinear focusing lens for the weak signal laser beam. As a result, the far-field diffraction ring patterns of the signal laser beam interacted with atoms can effectively carry the nonlinear phase shift information of the switch laser beam. The channel numbers, channel capacities and channel storage densities of information transmission from switch laser beam to signal laser beam are investigated in the terms of switch laser intensity and vapor temperature. Finally, a special "*sxu*" alphabetic string, encoded by ASCII code, is introduced to verify this all-optical information conversion scheme. This work paves the way for studying optical information processing and all-optical networking with atomic ensembles.

1. Introduction

All-optical information conversion processes signal from one channel to another by optical control approach instead of the electrical domain [1,2]. The requirements for data transmission with large capacity, high speed rate, and low power consumption accelerate the development of all-optical information conversion in the fields of all-optical data processing, all-optical devices, and optical communication [3–6]. Compared with the widely used linear mechanisms such as light-collimation effect and light beam interference effect [7–9], the nonlinear mechanisms based on four-wave mixing [10] and spatial cross-phase modulation [11] provide practical advantages of large capacity, wide broadband, and strong integration for all-optical information conversion [12].

Spatial cross-phase modulation, in which the spatial intensity of a laser beam is rearranged by Kerr nonlinear effect, is employed for all-optical information conversion as an excellent manifestation of nonlinear optical response [13]. When the switch laser beam interacts with the medium, the laser phase is modulated due to the change of the medium refractive index [14]. As a result, the phase of signal laser passing through the medium is reconstructed synchronously. In other words, the information of the switch laser beam is effectively transferred to the signal laser beam based on spatial cross-phase modulation in nonlinear medium.

The exotic nonlinear two-dimensional materials, such as graphene, $TaSe_2$ nanosheets, $NbSe_2$ nanosheets, and GeSe nanoflakes, have been applied as carriers for achieving all-optical information conversion based on spatial cross-phase modulation [15–22]. On the other hand, the atomic vapor with typical nonlinear effects of electromagnetically induced transparency, self-focusing, self-trapping, and spatial cross-phase modulation gradually began to be explored as

#476336 https://doi.org/10.1364/OE.476336
Journal © 2022 Received 23 Sep 2022; accepted 15 Nov 2022; published 30 Nov 2022

Optics EXPRESS

the candidate medium [23–30]. Recently, the spatial cross-phase modulation in atomic medium has been utilized for the generations of parameter-variable Bessel-like beam [31], dark-hollow beam [32], and high-order Bessel-like beam carrying orbital angular momentum [33]. Compared with two-dimensional materials, the flexible tunability and high damage threshold of atomic medium give more prospects in all-optical applications. To our best knowledge, the all-optical information conversion in atomic medium based on spatial cross-phase modulation has not been investigated experimentally.

In this work, we experimentally achieve the all-optical information conversion in Rb vapor based on spatial cross-phase modulation. The signal laser beam passing through the nonlinear atomic medium is phase modulated by the strongly focused switch laser beam. The nonlinear phase shift of switch laser beam is effectively transferred to the signal laser beam by observing the images of the far-field diffraction ring patterns. Meanwhile, the channel numbers, channel capacities and channel storage densities of information transmission are investigated with different laser intensities and Rb vapor temperatures. Furthermore, the special "*sxu*" alphabetic string, loaded on the switch laser beam encoding by ASCII code, is read out with high-fidelity from the signal laser beam to effectively confirm this all-optical information conversion scheme. This work provides a demonstration of atomic vapor-based all-optical devices, which have potential in all-optical networks and optical communication.

2. Experimental setup

The experimental setup for achieving the all-optical information conversion in Rb atoms is presented in Fig. 1(a). The switch and signal lasers, which are provided by the external cavity diode lasers (DL pro, Toptica), drive ^{85}Rb atoms transition from the ground state $5S_{1/2}(F = 3)$ to excited state $5P_{3/2}(F' = 4)$, where Δ_1 and Δ_2 represent frequency detunings of switch and signal laser beams, respectively [see Fig. 1(b)]. The strong switch laser beam, whose profile is monitored by a charge coupled device (CCD2), is focused through a lens (L) with focal length of 100 mm. A rubidium vapor cell with $10 \times 10 \times 10$ mm^3 is placed at the focus position of the switch laser beam. The weak signal laser beam overlaps with switch laser beam in the vapor cell by a counter-propagating configuration. The temperature of vapor is accurately controlled through a self-feedback system. Meanwhile, an acousto-optic modulator (AOM) is used to modulate the amplitude of switch laser beam for information loading. Finally, the signal laser beam profile passing through the vapor cell is detected by CCD1 for exploring the all-optical information conversion.

Figure 1(c) shows the schematic diagram of all-optical information conversion based on spatial cross-phase modulation. The nonlinear effect of the Rb atoms is excited by the focused switch laser beam and serves as a nonlinear focusing lens. The phase of signal laser beam is effectively spatially modulated after passing through the atomic medium. Therefore, the information of switch laser beam can be directly depicted on the signal laser beam for realizing information transmission.

Optics EXPRESS

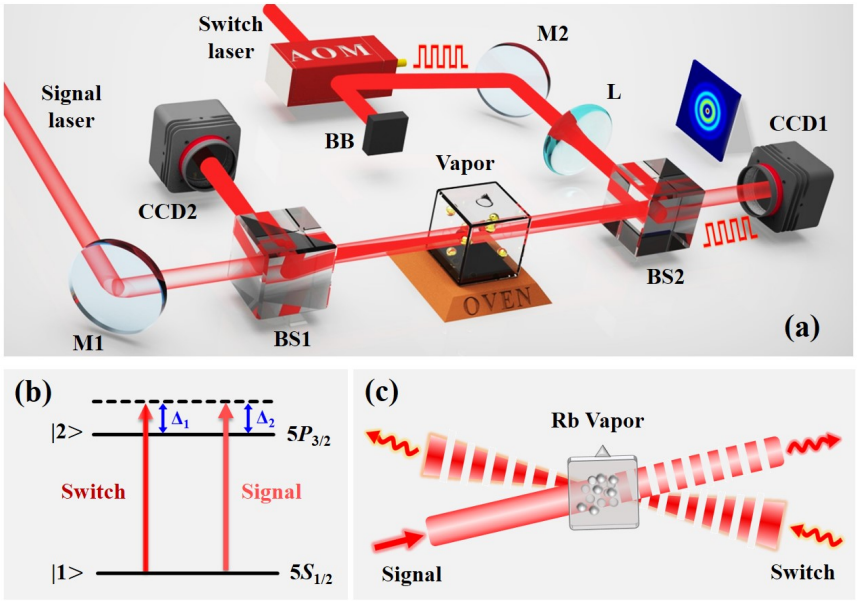

Fig. 1. (a) Sketch of the experimental setup. AOM, acousto-optic modulator; BB, beam block; M, high-reflection mirror; L, lens; BS, beam splitter; CCD, charge coupled device. (b) Relevant energy-level configuration of Rb atoms. (c) Schematic diagram for realizing the all-optical information conversion based on spatial cross-phase modulation.

3. Experimental results and discussions

The electric field distribution of input signal laser beam propagating along the z-axis direction is expressed as [34,35]:

$$E(r, z_0) = E(0, z_0) exp(-\frac{r^2}{\omega_p^2}) exp(-\frac{ikr^2}{2R(z)}) \tag{1}$$

where r is the radial coordinate, z_0 is the position coordinate of the medium entrance plane, $E(0, z_0)$ is the electric field of the entrance-plane center of the medium, $\omega_p = \omega_0(1 + z^2/{z_R}^2)^{1/2}$ is the spot size of the beam at the z position, $z_R = \pi\omega_0^2/\lambda$ is the diffraction length, ω_0 is the waist radius, $k = 2\pi/\lambda$ is the wave vector, and $R(z) = z + z_R^2/z$ is the curvature radius of the wave front.

When a strong switch laser beam propagated through the nonlinear medium with a length of L, the nonlinear effect of medium is induced by the spatial cross-phase modulation, which makes the refractive index is spatially modulated. The weak signal laser beam carries nonlinear phase shift in the radial direction on the exit of the nonlinear medium [33]. The order of magnitude intensity ratio between switch laser beam I_1 and signal laser beam I_2 makes the switch laser beam play a dominant role in spatial cross-phase modulation process. Therefore, the nonlinear phase shift of signal laser beam is expressed as [35]:

$$\phi_{signal}(r) = \Delta\phi_{signal} \exp(-\frac{2r^2}{\omega_p^2}) \tag{2}$$

where $\Delta\phi_{signal} = 2kn_2LI_1$ is peak nonlinear phase of signal laser beam, which is twice larger than the peak nonlinear phase of switch laser beam $\Delta\phi_{switch} = kn_2LI_1$, $n_2 \propto \frac{\mu_{12}^4 N}{2c\varepsilon_0^2 h^3 \Delta^3}$ is nonlinear refractive index of the medium [31], μ_{12} denotes the dipole matrix element, N is the atomic

Optics EXPRESS

number density, and Δ is the frequency detuning. Clearly, the nonlinear phase shift can be significantly adjusted by switch laser intensity and atomic number density.

Finally, the corresponding output far-field intensity distribution of switch and signal laser beams can be expressed by means of the Fraunhofer approximation of the Fresnel–Kirchhoff diffraction formula [36,37]:

$$I_{switch(signal)} = |\frac{1}{i\lambda D}|^2| \int_0^{\infty} \int_0^{2\pi} E(0, z_0) exp(-ikr\theta \cos\varphi) \times exp[-i(\frac{kr^2}{2R(z)} + \phi_{switch(signal)}(r)]rdrd\varphi|^2 \quad (3)$$

where D is the distance from the medium exit plane to the far-field observation plane, θ is the far-field diffraction angle, φ is the angular coordinate on the exit plane of the medium.

The far-field diffraction intensity distributions of switch and signal laser beams are theoretically simulated when the peak nonlinear phase shift $\Delta\phi_{switch}$ is 0, π and 2π, respectively, which are shown in Fig. 2. It can be seen that no diffraction occurs when the $\Delta\phi_{switch} = 0$, and the switch and signal laser beams passing through the medium shows the original Gaussian profiles as shown in Fig. 2(a). Furthermore, the diffraction rings are excited with the $\Delta\phi_{switch}$ increasing, which are illustrated in Figs. 2(b) and 2(c). The maximum intensity of the diffraction pattern locates at the center position due to the positive nonlinearity of the medium. When the $\Delta\phi_{switch} = \pi$, a weak ring is induced in the far-field diffraction pattern of the switch laser beam, while the signal laser beam exhibits two diffraction rings [see Fig. 2(b)] because the $\Delta\phi_{signal} = 2\Delta\phi_{switch}$ [31]. Furthermore, more diffraction rings of switch and signal laser beams are observed simultaneously with $\Delta\phi_{switch} = 2\pi$ as shown in Fig. 2(c), which indicates that more channels are obtained for information transmission.

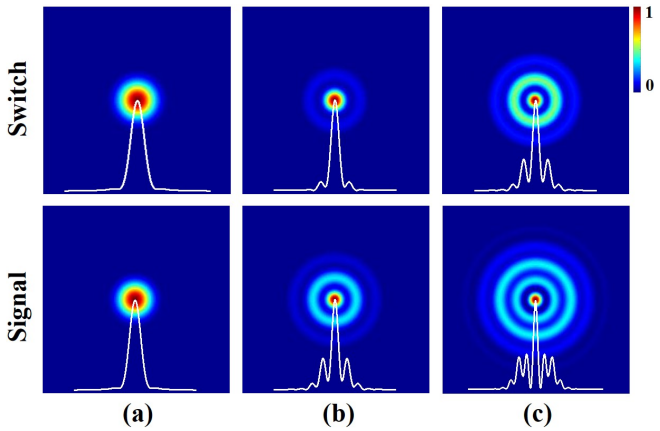

Fig. 2. The theoretical simulations of the output switch and signal laser beams profiles when the $\Delta\phi_{switch}$ is (a) 0, (b) π, and (c) 2π, respectively. The white curves below represent the spatial intensity distribution of the corresponding diffraction patterns.

The channel numbers, channel capacities and channel storage densities of all-optical information conversion can be adjusted by the nonlinear phase shift, which is influenced by the switch laser intensity and vapor temperature. Figure 3(a) describes the far-field diffraction profiles of switch and signal laser beams with different switch laser intensities. The Rb vapor temperature is kept at 140 °C. The frequency detunings of switch and signal laser beams are about 0.7 GHz from $5S_{1/2}(F = 3)$ - $5P_{3/2}(F' = 4)$ hyperfine transition. The signal laser intensity is fixed at 0.4 W/cm^2, which is lower than the threshold value for exciting the nonlinear effect of Rb atoms [38]. It can

Optics EXPRESS

be found that the switch laser beam behaves as a non-Gaussian profile with a central spot and a concentric diffraction ring when the intensity is 16 W/cm^2. Meanwhile, the diffraction rings of signal laser beam are synchronously excited. The number of signal laser beam diffraction rings is more than that of switch laser beam for the twice nonlinear phase shift of signal laser beam compared to the switch laser beam. As the switch laser intensity further increasing, the number of diffraction rings for both beams all synchronously increases, which means that the channel numbers of information transmission are increased.

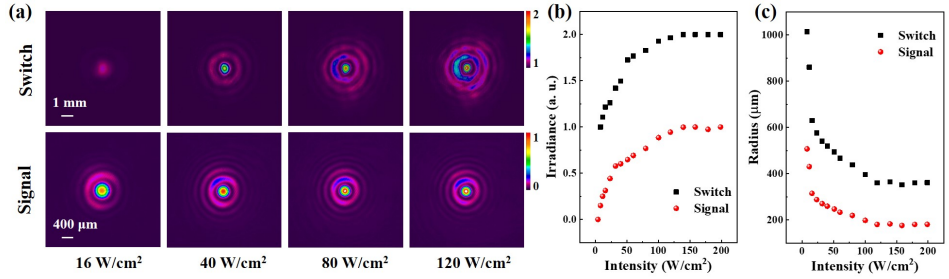

Fig. 3. (a) The far-field diffraction profiles of the switch and signal laser beams with switch laser intensities of 16, 40, 80, and 120 W/cm^2, respectively. The whole irradiance (b) and the central spot radius (c) of the switch and signal laser beams diffraction patterns with different switch laser intensities.

The whole irradiance of the diffraction profiles, characterizing the total channel capacity of information transmission, with different switch laser intensities are shown in Fig. 3(b). The whole irradiance of switch (black dots) and signal (red dots) laser beams diffraction profiles increase simultaneously with the increasing switch laser intensity for the increased nonlinear phase shifts, which is beneficial to the optical information transmission with large capacity. In addition, the central spot radius of the switch (black dots) and signal (red dots) laser beams diffraction profiles, describing the channel storage density, are synchronously reducing with the increasing switch laser intensity due to the enhanced focusing effect, which is shown in Fig. 3(c).

The intensity profiles of switch and signal far-field diffraction beams versus different vapor temperatures are shown in Fig. 4(a). The switch laser intensity is set at 60 W/cm^2. The vapor temperature is varied from 100 to 150 °C. The other experimental parameters are the same as in Fig. 3(a). The switch and signal laser beams behave weak diffraction rings profiles with the vapor temperature of 100 °C. When the vapor temperature is increased, more obvious diffraction rings of switch and signal laser beams are observed synchronously because the nonlinear phase shifts become larger, which indicates more channel numbers of information transmission are obtained. In addition, the whole irradiance of switch (black dots) and signal (red dots) laser beams diffraction profiles increases simultaneously with the increasing vapor temperature as shown in Fig. 4(b), indicating expanded total channel capacity of information transmission. Moreover, the center spot radius decreases simultaneously for the enhanced focusing strength of switch and signal laser beams diffraction profiles as shown in Fig. 4(c), which means the increasing channel storage density.

To verify the all-optical information conversion in Rb vapor based on spatial cross-phase modulation, a specific information compiled digitally by binary ASCII code is loaded into the switch laser beam, and is read out by detecting the output signal laser beam passing through the vapor cell, which is shown in Fig. 5. The transmitted "*sxu*" alphabetic string is converted into "01110011 01111000 01110101" ASCII code. The obtained ASCII code is loaded on the input switch laser beam (red line) while the input signal laser beam (blue line) always maintains the same "1" state, as shown in Fig. 5(a). The "1" and "0" states of the input switch laser beam are controlled by the amplitude modulation using the AOM. The information reading out is

Optics EXPRESS

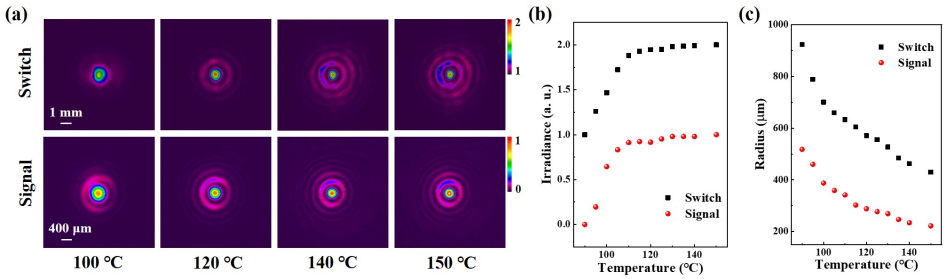

Fig. 4. (a) The diffraction profiles of switch and signal laser beams with Rb vapor temperatures of 100, 120, 140 and 150 °C, respectively. The whole irradiance (b) and the central spot radius (c) of the switch (black dots) and signal (red dots) laser beams diffraction profiles at different vapor temperatures.

realized by the output outermost diffraction rings of the far-field diffraction profiles intensity via photodetectors combining with the apertures. It can be found that the "*sxu*" alphabetic string is reproduced on the output beams with strict time synchronization and accuracy as shown in Fig. 5(b). Therefore, the information of the switch laser beam is high-fidelity written on the signal laser beam for achieving all-optical information conversion.

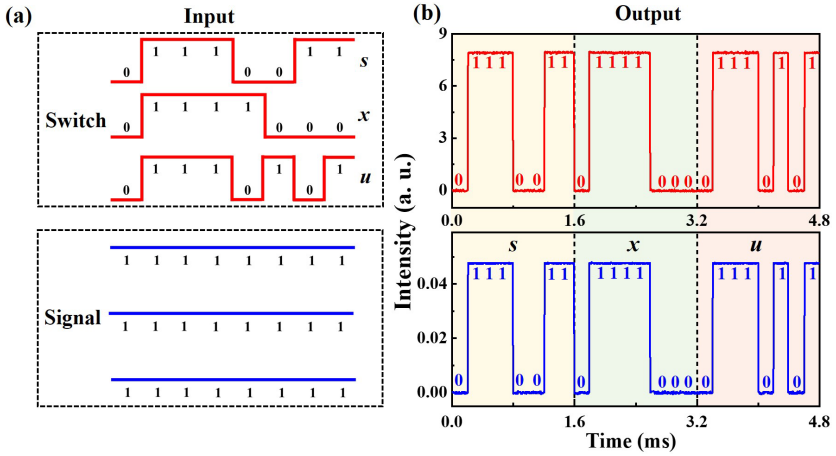

Fig. 5. The all-optical information conversion from switch laser beam to signal laser beam. (a) The input ASCII code for loading on switch and signal laser beams. (b) The corresponding output switch and signal laser beams.

4. Conclusions

In summary, we have achieved the all-optical information conversion in Rb vapor based on the spatial cross-phase modulation. The atomic medium, serves as a nonlinear focusing lens, is modulated by the strong switch laser beam. The weak signal laser beam undergoes a nonlinear phase shift after passing through the atomic medium. Thereby, the output signal laser beam with far-field diffraction ring patterns is applied to effectively carry the nonlinear phase shift of switch laser beam. The channel numbers, channel capacities and channel storage densities for information transmission from switch laser beam to signal laser beam are flexibly adjusted by the switch laser intensity and vapor temperature. Furthermore, the transmission of the specific "*sxu*" alphabetic string, encoded by ASCII code, from switch laser beam to signal laser beam is

Optics EXPRESS

achieved to verify this all-optical information conversion scheme. The realization method of all-optical application is useful for optical information processing and all-optical networking proposed in atomic ensembles.

Funding. National Natural Science Foundation of China (61875112, 62075121); the Program for Sanjin Scholars of Shanxi Province; Key Research and Development Program of Shanxi Province for International Cooperation (201803D421034); Shanxi 1331 Project; Open Fund of MOE Key Laboratory of Weak-Light Nonlinear Photonics (OS 22-2).

Disclosures. The authors declare no conflicts of interest.

Data availability. Data underlying the results presented in this paper are not publicly available at this time but may be obtained from the authors upon reasonable request.

References

1. L. Wu, X. Jiang, J. Zhao, W. Liang, Z. Li, W. Huang, Z. Lin, Y. Wang, F. Zhang, S. Lu, Y. Xiang, S. Xu, J. Li, and H. Zhang, "MXene-based nonlinear optical information converter for all-optical modulator and switcher," Laser Photonics Rev. **12**(12), 1800215 (2018).
2. H. Chena, C. Wanga, H. Ouyang, Y. Song, and T. Jiang, "All-optical modulation with 2D layered materials: status and prospects," Nanophotonics **9**(8), 2107–2124 (2020).
3. L. Stern, B. Desiatov, N. Mazurski, and U. Levy, "Strong coupling and high-contrast all-optical modulation in atomic cladding waveguides," Nat. Commun. **8**(1), 14461 (2017).
4. J. Yuan, S. Dong, H. Zhang, C. Wu, L. Wang, L. Xiao, and S. Jia, "Efficient all-optical modulator based on a periodic dielectric atomic lattice," Opt. Express **29**(2), 2712–2719 (2021).
5. W. Li, B. Chen, C. Meng, W. Fang, Y. Xiao, X. Li, Z. Hu, Y. Xu, L. Tong, and H. Wang, "Ultrafast all-optical graphene modulator," Nano Lett. **14**(2), 955–959 (2014).
6. J.-H. Chen, B.-C. Zheng, G.-H. Shao, S.-J. Ge, F. Xu, and Y.-Q. Lu, "An all-optical modulator based on a stereo graphene-microfiber structure," Light: Sci. Appl. **4**(12), e360 (2015).
7. Y.-C. Jiang, S.-B. Liu, H.-F. Zhang, and X.-K. Kong, "Realization of all optical half-adder based on self-collimated beams by two-dimensional photonic crystals," Opt. Commun. **348**, 90–94 (2015).
8. K. Ogusu, "All-optical switching in nonlinear multimode interference couplers," Jpn. J. Appl. Phys. **51**, 082503 (2012).
9. M. Sen and M. K. Das, "High-speed all-optical logic inverter based on stimulated Raman scattering in silicon nanocrystal," Appl. Opt. **54**(31), 9136–9142 (2015).
10. G. M. Fernandes, A. M. Rocha, and M. Facão, "Mode switching using optically induced long-period gratings: a theoretical analysis," Opt. Express **29**(10), 14601–14614 (2021).
11. Y. Jia, Y. Liao, L. Wu, Y. Shan, X. Dai, H. Cai, Y. Xiang, and D. Fana, "Nonlinear optical response, all optical switching, and all optical information conversion in $NbSe_2$ nanosheets based on spatial self-phase modulation," Nanoscale **11**(10), 4515–4522 (2019).
12. V. Sasikala and K. Chitra, "All optical switching and associated technologies: a review," J. Opt. **47**(3), 307–317 (2018).
13. L. Wu, Y. Dong, J. Zhao, D. Ma, W. Huang, Y. Zhang, Y. Wang, X. Jiang, Y. Xiang, J. Li, Y. Feng, J. Xu, and H. Zhang, "Kerr nonlinearity in 2D graphdiyne for passive photonic diodes," Adv. Mater. **31**(14), 1807981 (2019).
14. L. Cheng, Z. Zhang, L. Zhang, D. Ma, G. Yang, T. Dong, and Y. Zhang, "Manipulation of a ring-shaped beam via spatial self- and cross-phase modulation at lower intensity," Phys. Chem. Chem. Phys. **21**(14), 7618–7622 (2019).
15. S. Liu, J. Han, X. Cheng, X. Wang, Q. Zhang, B. He, T. Jiao, and Z. Ren, "Mechanism of all-optical spatial light modulation in graphene dispersion," J. Phys. Chem. C **125**(30), 16598–16604 (2021).
16. Y. Shan, L. Wu, Y. Liao, J. Tang, X. Dai, and Y. Xiang, "A promising nonlinear optical material and its applications for all-optical switching and information converters based on the spatial self-phase modulation (SSPM) effect of $TaSe_2$ nanosheets," J. Mater. Chem. C **7**(13), 3811–3816 (2019).
17. Y. Jia, Z. Li, M. Saeed, J. Tang, H. Cai, and Y. Xiang, "Kerr nonlinearity in germanium selenide nanoflakes measured by Z-scan and spatial self-phase modulation techniques and its applications in all-optical information conversion," Opt. Express **27**(15), 20857–20873 (2019).
18. Y. Liao, C. Song, Y. Xiang, and X. Dai, "Recent advances in spatial self-phase modulation with 2d materials and its applications," Ann. Phys. **532**(12), 2000322 (2020).
19. G. Wang, S. Zhang, X. Zhang, L. Zhang, Y. Cheng, D. Fox, H. Zhang, J. N. Coleman, W. J. Blau, and J. Wang, "Tunable nonlinear refractive index of two-dimensional MoS_2, WS_2, and $MoSe_2$ nanosheet dispersions," Photonics Res. **3**(2), A51–A55 (2015).
20. L. Lu, W. Wang, L. Wu, X. Jiang, Y. Xiang, J. Li, D. Fan, and H. Zhang, "All-optical switching of two continuous waves in few layer bismuthene based on spatial cross-phase modulation," ACS Photonics **4**(11), 2852–2861 (2017).
21. Y. Liao, Q. Ma, Y. Shan, J. Liang, X. Dai, and Y. Xiang, "All-optical applications for passive photonic devices of TaS_2 nanosheets with strong Kerr nonlinearity," J. Alloys Compd. **806**, 999–1007 (2019).

Optics EXPRESS

22. L. Wu, X. Yuan, D. Ma, Y. Zhang, W. Huang, Y. Ge, Y. Song, Y. Xiang, J. Li, and H. Zhang, "Recent advances of spatial self-phase modulation in 2D materials and passive photonic device applications," Small **16**(35), 2002252 (2020).
23. S. Ning, J. Lu, S. Liang, Y. Feng, C. Li, Z. Zhang, and Y. Zhang, "Talbot effect of an electromagnetically induced square photonic lattice assisted by a spatial light modulator," Opt. Lett. **46**(19), 5035–5038 (2021).
24. H. Hu, D. Luo, C. Pan, Y. Qin, Y. Zhang, D. Wei, H. Chen, H. Gao, and F. Li, "Collapse of hybrid vector beam in Rb atomic vapor," Opt. Lett. **46**(11), 2614 (2021).
25. Z. Zhang, S. Liang, F. Li, S. Ning, Y. Li, G. Malpuech, Y. Zhang, M. Xiao, and D. Solnyshkov, "Spin–orbit coupling in photonic graphene," Optica **7**(5), 455–462 (2020).
26. H. Cai, J. Liu, J. Wu, Y. He, S.-Y. Zhu, J.-X. Zhang, and D.-W. Wang, "Experimental observation of momentum-space chiral edge currents in room-temperature atoms," Phys. Rev. Lett. **122**(2), 023601 (2019).
27. Z. Zhang, R. Wang, Y. Zhang, Y. V. Kartashov, F. Li, H. Zhong, H. Guan, K. Gao, F. Li, Y. Zhang, and M. Xiao, "Observation of edge solitons in photonic graphene," Nat. Commun. **11**(1), 1902 (2020).
28. S. Wang, J. Yuan, L. Wang, L. Xiao, and S. Jia, "Measurement of the Kerr nonlinear refractive index of the Rb vapor based on an optical frequency comb using the z-scan method," Opt. Express **28**(25), 38334–38342 (2020).
29. C. P. Jisha, A. Alberucci, J. Beeckman, and S. Nolte, "Self-trapping of light using the pancharatnam-berry phase," Phys. Rev. X **9**(2), 021051 (2019).
30. J. Wu, M. Guo, H. Zhou, J. Liu, J. Li, and J. Zhang, "Experimental realization of efficient nondegenerate four-wave mixing in cesium atoms," Opt. Express **30**(8), 12576–12585 (2022).
31. X. Cheng, Q. Zhang, H. Chen, B. He, Z. Ren, Y. Zhang, and J. Bai, "Demonstration of Bessel-like beam with variable parameters generated using cross-phase modulation," Opt. Express **25**(21), 25257–25266 (2017).
32. Q. Zhang, X. Cheng, B. He, H. Chen, Z. Ren, and J. Bai, "Size-variable dark-hollow beam generation using cross-phase modulation," Opt. Laser Technol. **119**, 105582 (2019).
33. J. Yuan, X. Wang, L. Wang, L. Xiao, and S. Jia, "Tunable high-order Bessel-like beam generation based on cross-phase modulation," Opt. Express **30**(10), 15978–15985 (2022).
34. A. G. Nibu, S. S. Silpa, S. N. Ardra, M. M. Anisha, and D. Ambika, "Effect of viscosity on the far-field diffraction pattern of spatial SPM," Opt. Appl. **47**, 591–599 (2017).
35. T. Neupane, B. Tabibi, and F. J. Seo, "Spatial self-phase modulation in WS_2 and MoS_2 atomic layers," Opt. Mater. Express **10**(4), 831–842 (2020).
36. L. Deng, K. He, T. Zhou, and C. Li, "Formation and evolution of far-field diffraction patterns of divergent and through self-focusing and self-defocusing media," J. Opt. A: Pure Appl. Opt. **7**(8), 409–415 (2005).
37. Y. Zhang, X. Cheng, X. Yin, J. Bai, P. Zhao, and Z. Ren, "Research of far-field diffraction intensity pattern in hot atomic Rb sample," Opt. Express **23**(5), 5468–5476 (2015).
38. C. F. McCormick, D. R. Solli, R. Y. Chiao, and J. M. Hickman, "Saturable nonlinear refraction in hot atomic vapor," Phys. Rev. A **69**(2), 023804 (2004).